EXPERIMENTAL RESULTS ON POLARIZED NUCLEON STRUCTURE FUNCTIONS*

T.J. Ketel

for the Spin Muon Collaboration at CERN

Department of Physics and Astronomy, Free University
1081 HV Amsterdam, The Netherlands

(Received April 12, 1998)

Experimental results of deep inelastic scattering of polarized leptons from polarized target nucleons are reviewed. Accurate values of the spin dependent structure function $g_1(x)$ were obtained in experiments covering a large kinematic range. The combination of all experimental results confirms the validity of the Bjorken sum rule.

PACS numbers: 12.38. Qk

1. Introduction

During the last decade experiments of polarized deep inelastic lepton scattering were focused on the spin dependent structure function $g_1(x)$ and its first moment Γ_1. The main issues were the earlier observed deviation from the Ellis-Jaffe sum rule [1, 2] and the validity of the Bjorken sum rule [3]. Both at SLAC and at CERN experimental groups collected vast amounts of data within the limits of their experimental set-ups. This resulted in high quality data sets in overlapping kinematic domains which, to the delight of the community involved, were consistent which each other and allowed for a QCD analysis of $g_1(x, Q^2)$ (see Refs [4–6]). The richness of the information which can be obtained from a QCD analysis of g_1 is in principle larger than that of the structure function F_2. However, the experimental data on g_1 is yet more limited in statistical accuracy and kinematic range. It should be part of a future program for spin effects in particle physics to determine g_1 with improved accuracy over a larger x and Q^2 range, if possible, at the HERA collider with polarized nuclei.

* Presented at the Cracow Epiphany Conference on Spin Effects in Particle Physics and Tempus Workshop, Cracow, Poland, January 9–11, 1998.

2. Experiments

Experiments of deep inelastic lepton nucleon scattering with polarized beams and polarized targets are summarized in Table I. The energy of the electron or muon beam determines the smallest value of the Bjorken x variable obtainable with a four-momentum transfer corresponding to $Q^2 > 1$ GeV^2. The kinematic acceptances of SLAC and CERN experiments are shown in Fig. 1.

TABLE I

Comparison of the kinematics for the different g_1 experiments

Experiment	beam	E (GeV)	smallest x $Q^2 > 1$ GeV^2	average Q^2 (GeV^2)	target nucleon
E-80/130	e$^-$	23	0.10	4	p
EMC	μ^+	100–200	0.01	10.7	p
SMC	μ^+	100–190	0.003	10	p,d
E-142	e$^-$	19–25	0.03	2	n
E-143	e$^-$	10–29	0.029	3	p,d
E-154	e$^-$	48.3	0.014	5	n
E-155	e$^-$	48.3	0.014	5	p,d
HERMES	e$^+$	27.5	0.023	2.3	n,p,d

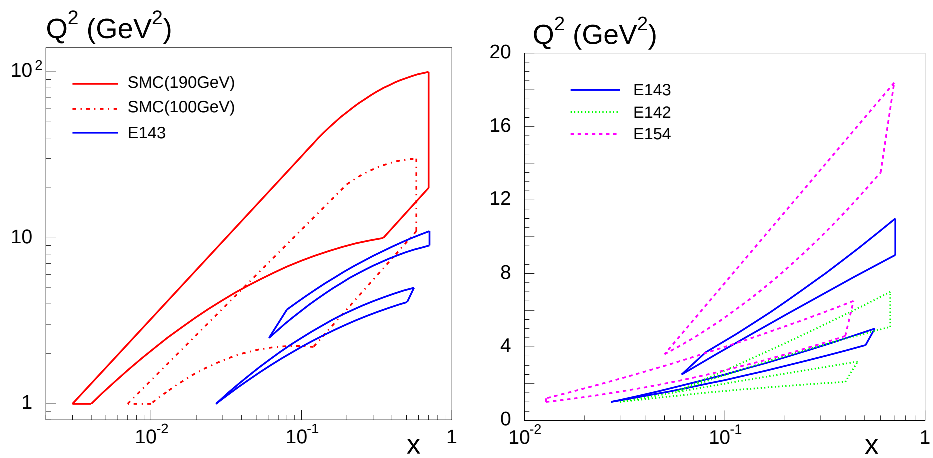

Fig. 1. Kinematic ranges in x and Q^2 covered by the SMC and recent SLAC experiments.

2.1. E142-155 at SLAC

In the SLAC experiments magnetic spectrometers at different forward angles were used to measure the scattered electrons. High beam polarizations up to $P_b = 0.80$ were obtained by using strained GaAs crystals as polarized electron sources. The sign of the polarization was randomly selected for each beam pulse. The targets used by E142 and E154 were high pressure ^{3}He gas cells, while E143 and E155 used frozen ammonia with enriched ^{15}N and hydrogen or deuterium ($^{15}NH_3$, $^{15}ND_3$). The polarization of the gas targets was obtained by optical pumping and for the solid targets dynamic nuclear polarization (DNP) was used.

2.2. HERMES at DESY

The HERMES experiment used internal gas targets of polarized atomic hydrogen, deuterium and ^{3}He, and the high current longitudinally polarized positron beam of the HERA collider at DESY. The beam was polarized by the Sokolov–Ternov effect with an average value of $P_{\rm b} = 0.55$. The forward spectrometer accepted scattering angles of $40 < \Theta < 220$ mrad and provided efficient positron identification and track reconstruction.

2.3. SMC at CERN

The SMC spectrometer consisted of a forward spectrometer magnet and muon identification within the acceptance of $3 < \Theta < 150$ mrad. The muon beam polarimeter used the muon decay method, which examined the energy spectrum of the positrons originating from muon decays, and the scattering asymmetry from longitudinally polarized electrons in a magnetized foil to determine the beam polarization $P_{\rm b} = 0.80$. The target consisted of a double cell setup with frozen (deuterated) butanol or ammonia material polarized by DNP in opposite directions for the two cells and exposed simultaneously to the full muon beam. Vertex reconstruction was used to select the events from either target cell.

3. Spin asymmetries

The world data on the spin asymmetries $A_1(x)$ and $A_2(x)$ are shown in Figs. 2 and 3. The data were published by EMC [1], SMC [7, 8], E142 [9], E143 [10], E154 [11], and HERMES [12].

Measured count rate asymmetries for opposite longitudinal beam or target polarizations were used to determine the virtual photon asymmetry $A_1(x)$, where the count rate

$$N = n\phi a\bar{\sigma}\{1 - fDP_{\rm b}P_t(A_1 + \eta A_2)\} \qquad (1)$$

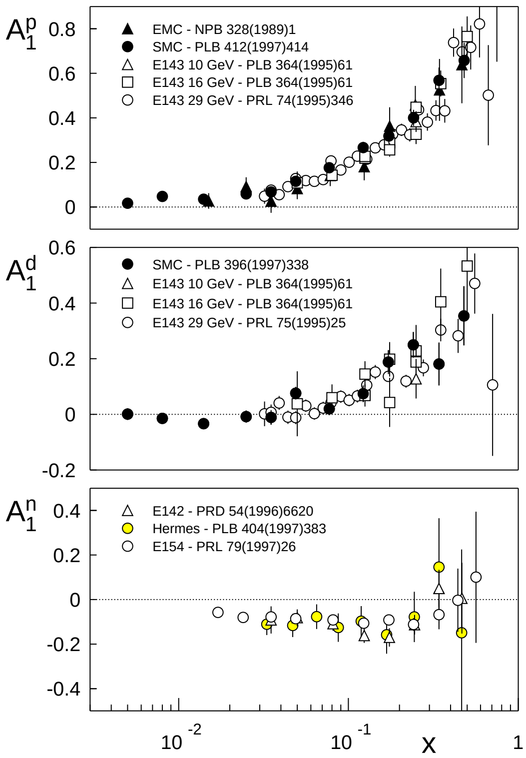

Fig. 2. World data on $A_1^{\rm p}$, $A_1^{\rm d}$ and $A_1^{\rm n}$. The errors are statistical.

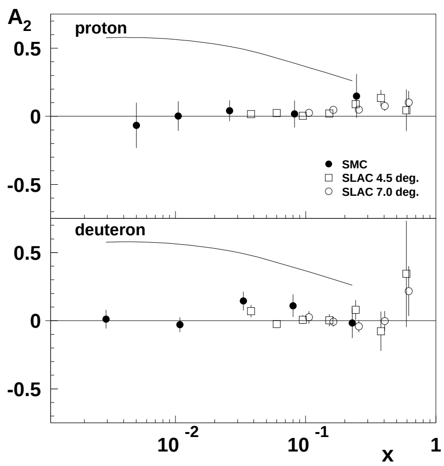

Fig. 3. World data on $A_2^{\rm p}$ and $A_2^{\rm d}$. The upper limit of $\sqrt{R}$ is plotted for the SMC kinematics. The errors are statistical.

depends on the target density per cm^2, n, the beam flux ϕ, the detector acceptance a, the unpolarized cross section $\bar{\sigma}$, the dilution factor f, the depolarization factor D, the beam polarization P_{b}, the target polarization P_t, a small kinematic factor η, and the spin asymmetries A_1 and A_2. The uncertainties due to n, ϕ, a and $\bar{\sigma}$ canceled to a large extend by the way the experiments were carried out and analysed.

4. Evaluation of g_1 and its first moment

In the SMC analysis the spin dependent structure function $g_1(x, Q^2)$ was determined from the measured spin asymmetries $A_1(x, Q^2)$ and a parameterization of the structure functions F_2 and R. A next-to-leading order QCD analysis of the world proton data was used to evolve the measured $g_1(x, Q^2)$ to a fixed value of Q_0^2.

In Fig. 4 the results show significant differences between the values of $g_1^p(x)$ for the SLAC and SMC kinematics due to the higher values of Q^2 in the SMC experiment. Those differences are entirely due to the scaling violation of $F_2^p(x)$, as the spin asymmetries $A_1^p(x)$ in Fig. 2 show perfect overlap for the experiments at different Q^2. If the strong coupling parameter α_S is left as a free parameter in the QCD fit, its value and accuracy will, therefore, be determined by the chosen parameterization of $F_2(x, Q^2)$ and not so much by the measured spin asymmetries $A_1(x, Q^2)$.

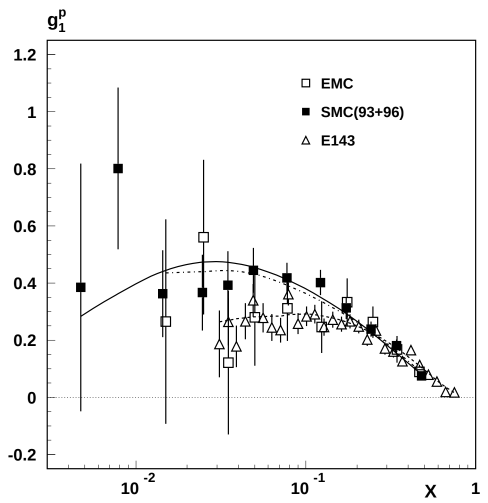

Fig. 4. The proton structure function data $g_1^p(x)$ compared with the result of the NLO QCD fit plotted for the average Q^2 of each x bin of the EMC, SMC and E143 experiments.

The first moment $\Gamma_1^p = \int_0^1 g_1^p(x)\, dx$ was determined at the average Q^2 of the SMC measurement, $Q_0^2 = 10$ GeV^2 [7]. For comparison with the world data we here discuss its value evaluated at $Q_0^2 = 5$ GeV^2. The contribution $I_{\rm m}$ to the first moment of g_1^p in the measured range $0.003 < x < 0.7$ was $I_{\rm m} = 0.134 \pm 0.006 \pm 0.008 \pm 0.007$, where the first error is statistical, the second is systematic, and the third is due to the QCD evolution. The contribution at large x was estimated $I_{\rm l} = 0.002 \pm 0.001$. To evaluate the contribution at small x two approximations were used. The first one was a Regge type behaviour for g_1^p, which yielded $I_{\rm s} = 0.002 \pm 0.002$. The other was the QCD fit used for the evaluation at Q_0^2, and here used for the extrapolation to small x yielding $I_{\rm s} = -0.011 \pm 0.011$. Both extrapolations are shown in Fig. 5.

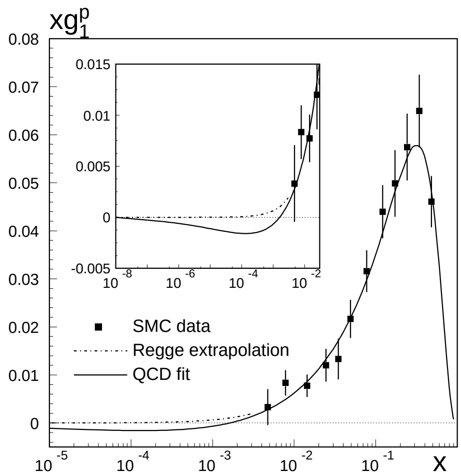

Fig. 5. The proton structure function $g_1^p(x)$ with Regge extrapolation and with the QCD fit.

In Table II the results for the first moments are given at the average Q^2 of the world data, $Q^2 = 5$ GeV^2. The quoted uncertainties are dominated by systematic contributions and underlines that further improvement of the results should come from a better understanding of the extrapolations and the reduction of other systematic error sources like the beam and target polarization uncertainties.

A publication [14] is in preparation with a complete and final analysis of the SMC data with an updated value for the beam polarization, based on both the muon decay method and polarized muon electron scattering, with more precise data obtained with hadron selection of deep inelastic events at small x, and a NLO QCD evaluation of $g_1(x,Q^2)$ over the full x range. New data from E-155 and HERMES for $g_1(x,Q^2)$ are expected to be published soon.

TABLE II

First moments $\Gamma_1 = \int_0^1 g_1(x)dx$ at $Q_0^2 = 5$ GeV^2 and errors due to (*i*) statistics, (*ii*) systematics and (*iii*) x and Q^2 extrapolations for the proton, deuteron and neutron (^{3}He). The combined results are with Regge extrapolation of $g_1(x)$ for $x \to 0$. The missing values anticipate the final results of SMC and the publications by E-155 and HERMES.

Γ_1^p		Γ_1^d		Γ_1^n	
EMC	0.128 (13) (18) (4)	SMC92	0.032 (21) (6) (8)	E-142^1	−0.032 (5) (11) (6)
SMC93	0.130 (13) (8) (7)	E143	0.042 (3) (4) (2)	E-154^2	−0.041 (4) (6) (6)
E-143	0.129 (3) (8) (7)	SMC94	0.038 (9) (3) (7)	E-154^3	−0.056 (4) (6) (2)
SMC96^2	0.140 (6) (8) (6)	SMC95	0.038 (8) (3) (7)	HERMES^4	−0.037 (13) (5) (6)
SMC96^3	0.128 (6) (8) (14)	SMC	–		
SMC	–				
E-155	–				
HERMES	–				
Combined^2	0.136 (9)		0.039 (6)		−0.054 (11)

$^{1)}$ at $Q^2 = 2$ GeV^2

$^{2)}$ Regge for small x

$^{3)}$ QCD fit for small x

$^{4)}$ at $Q^2 = 2.5$ GeV^2

5. Bjorken and Ellis–Jaffe sum rules

The combined first moments of $g_1(x)$ for the proton, neutron and deuteron are shown in Fig. 6 as bands of one standard deviation around their central values. The deuteron band is $\Gamma_1^p + \Gamma_1^n = 2\Gamma_1^d/(1 - \frac{3}{2}\omega_D)$, where ω_D

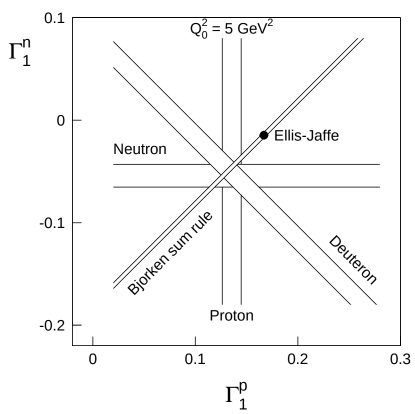

Fig. 6. The first moments of $g_1(x)$ at $Q_0^2 = 5$ GeV^2 for the proton, neutron and deuteron as given in Table 4, compared with the Bjorken, and Ellis–Jaffe predictions.

corresponds to the D-state contribution in the deuteron. The result for the first moment of g_1^p for the world data assuming Regge extrapolation, $\Gamma_1^p = 0.136 \pm 0.009$, violates the Ellis-Jaffe prediction of 0.167 ± 0.005 at $Q_0^2 = 5\,\mathrm{GeV}^2$ and in combination with the deuteron result, $\Gamma_1^d = 0.039 \pm 0.006$, confirms the Bjorken sum rule, $\Gamma_1^p - \Gamma_1^n = 0.190 \pm 0.017$, predicted as 0.181 ± 0.003.

If the axial charge contribution from strange sea quarks in the nucleon is allowed to be different from zero, contrary to the assumption of the Ellis–Jaffe sum rule, we find $a_u = 0.82 \pm 0.02$, $a_d = -0.44 \pm 0.02$, and $a_s = -0.10 \pm 0.02$, with the following conditions for the weak coupling constants $F + D = 1.260 \pm 0.003$ and $F/D = 0.575 \pm 0.016$.

Through the anomaly diagram the gluon spin contribution to the nucleon spin, ΔG, contributes to the measured axial charges with $a_q = \Delta q - \frac{\alpha_S}{2\pi}\Delta G$. A large gluon polarization with $\Delta G = 2.2 \pm 0.5$ could thus allow for an unpolarized strange sea with $\Delta s = 0$.

6. Polarized quark distributions

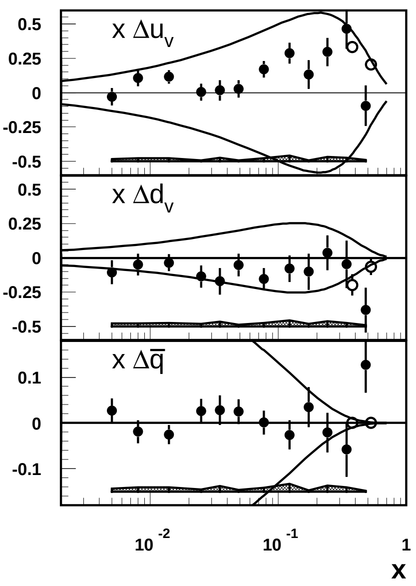

Fig. 7. Flavour separated polarized quark distributions $x\Delta q(x)$. The curves represent the upper and lower bounds given by the corresponding unpolarized distributions. The open circles at large x correspond to the restriction $|\Delta\bar{q}(x)| \leq \bar{q}(x)$. The size of the systematic uncertainty is indicated by the shaded bands.

Semi-inclusive spin asymmetries for positively and negatively charged hadrons from polarized protons and deuterons were analysed to determine the polarized valence quark distributions $\Delta u_v(x)$ and $\Delta d_v(x)$, as well as the polarized sea quark distribution $\Delta\bar{q}(x)$. The results shown in Fig. 7 were obtained by including the inclusive asymmetries in an analysis based on the quark parton model description of structure functions and fragmentation functions. Experimental fragmentation functions were measured by the EMC.

The polarization of the u_v quarks was found to be positive and to increase with x. The polarization of the d_v quarks was found to be negative. For the sea quarks ($\bar{u}$ and $\bar{d}$ in our analysis), the observed polarization was consistent with zero with high accuracy at small x. The first moments of the polarized quark distributions were $\Delta u_v = 0.77\pm0.10\pm0.08$, $\Delta d_v = -0.52\pm0.14\pm0.09$, and $\Delta\bar{q} = 0.010 \pm 0.04 \pm 0.03$, in good agreement with the axial charge contributions presented in the previous section.

7. Conclusions

The presented data sets of g_1 cover a substantial range in x for both g_1^p and g_1^d. The use of polarized ^{3}He as a polarized neutron target in the E142 and E154 experiments at SLAC and by HERMES at DESY provides direct measurements of g_1^n which are in good agreement with the combined proton and deuteron data.

The experimental results for the first moments $\Gamma_1^{p,d,n}$ confirm the validity of the Bjorken sum rule with an uncertainty of about 10 percent. The violation of the Ellis–Jaffe sum rule is clearly demonstrated and indicates either a large negative polarization of strange quarks in the nucleon or a large positive gluon spin contribution to the nucleon spin at a relatively low Q^2 scale.

Polarization distributions for up and down valence quarks are determined from semi-inclusive asymmetries in the framework of the quark parton model. Positive polarization of up valence quarks and negative polarization of down valence quarks in the proton are demonstrated, together with vanishing polarization of up and down sea quarks. More data on semi-inclusive neutron asymmetries are needed to improve the accuracy of the down valence quark polarization distribution and to test isospin symmetry of polarized parton distributions. The main purpose of the polarized semi-inclusive lepton nucleon scattering experiments of HERMES and COMPASS will be a direct measurement of the gluon polarization.

REFERENCES

[1] J. Ashman *et al.*, *Phys. Lett.* **B206**, 364 (1988); *Nucl. Phys.* **B328**, 1 (1989).

[2] J. Ellis, R.L. Jaffe, *Phys. Rev.* **D9**, 1444 (1974); **D10**, 1669 (1974).

[3] J.D. Bjorken, *Phys. Rev.* **148**, 1467 (1966); **D1**, 1376 (1970).

[4] T. Gehrmann, W.J. Stirling, *Phys. Rev.* **D53**, 6100 (1996).

[5] R.D. Ball, S. Forte, G. Ridolfi, *Phys. Lett.* **B378**, 255 (1996).

[6] M. Glück *et al.*, *Phys. Rev.* **D53**, 4775 (1996).

[7] SMC, D. Adams *et al.*, *Phys. Lett.* **B329**, 399 (1994); **B336**, 125 (1994); *Phys. Rev.* **D56**, 5330 (1997); B. Adeva *et al.*, *Phys. Lett.* **B412**, 414 (1997).

[8] SMC, B. Adeva *et al.*, *Phys. Lett.* **B302**, 533 (1993); D. Adams *et al.*, *Phys. Lett.* **B357**, 248 (1995); **B396**, 338 (1997).

[9] E142, D.L. Anthony *et al.*, *Phys. Rev. Lett.* **71**, 959 (1993); *Phys. Rev.* **D54**, 6620 (1996).

[10] E143, K. Abe *et al.*, *Phys. Rev. Lett.* **74**, 346 (1995); **75**, 25 (1995); **76**, 587 (1996); *Phys. Lett.* **B364**, 61 (1995).

[11] E154, K. Abe *et al.*, *Phys. Rev. Lett.* **79**, 26 (1997).

[12] HERMES, K. Ackerstaff *et al.*, *Phys. Lett.* **B404**, 383 (1997).

[13] SMC, D. Adams *et al.*, *Phys. Lett.* **B329**, 399 (1994); CERN-PPE/97-147, *Phys. Lett.* **B420**, 180 (1998).

[14] SMC, B. Adeva *et al.*, to be publ. in *Phys. Rev.* **D**.